

# Relaxation mechanism of GaP grown on 001 Si substrates: influence of defects on the growth of AlGaP layers on GaP/Si templates.

K. Pantzas<sup>a,\*</sup>, G. Beaudoin<sup>a</sup>, M. Bailly<sup>a,b</sup>, A. Martin<sup>b</sup>, A. Grisard<sup>b</sup>, D. Dolfi<sup>b</sup>,  
O. Mauguin<sup>a</sup>, L. Largeau<sup>a</sup>, I. Sagnes<sup>a</sup>, G. Patriarche<sup>a</sup>

<sup>a</sup>*Université Paris-Saclay, CNRS, Centre de Nanosciences et de Nanotechnologies - C2N, 91120, Palaiseau, France.*

<sup>b</sup>*Thales Research & Technology, F-91120, Palaiseau, France*

---

## Abstract

The mechanical stability of commercial GaP/Si templates during thermal annealing and subsequent MOCVD growth of GaP and AlGaP is investigated. Although the GaP layer of the template originally presents an excellent surface morphology, annealing at high enough temperatures to remove the native oxide prior to growth leads to plastic relaxation, accompanied by a variety of defects, including a dense grid of micro-twins. These micro-twins detrimentally affect GaP and AlGaP layers grown subsequently on the template.

---

## 1. Introduction

The (Al, Ga)P system possesses a significant number of properties highly desirable for nanophotonics integrated on Si. A non-exhaustive list of these properties includes: lattice mismatches of only 0.36 percent between GaP and Si [1], the smallest among all III-V compounds and Si, and 0.3 % between AlP and GaP, allowing for the growth of thick, high-quality layers and Bragg mirrors [2, 3]; a refractive index contrast as large as 0.4 at 700 nm and 0.57 at 500 nm. Only fifteen AlP/GaP pairs are, therefore, required to yield a peak reflectivity of 98 % for wavelengths between 530 nm to 690 nm [4]; band-gap energies of 2.5 eV

---

\*Corresponding author

*Email address:* [konstantinos.pantzas@c2n.upsaclay.fr](mailto:konstantinos.pantzas@c2n.upsaclay.fr) (K. Pantzas)

and 2.24 eV for AlP and GaP, respectively, making both materials transparent to the green-to-red region of the visible spectrum and allowing active structures to be optically pumped by conventional green lasers; high second-order nonlinearity, Pockels, and piezoelectric effects [3, 5]; high thermal conductivity,  $110 \text{ W K}^{-1} \text{ m}^{-1}$ , twenty times higher than that of active region material InGaP [6], and close to that of Si.

Despite both the low lattice and thermal mismatch between Si and the (Al, Ga)P system, their integration is not straightforward. Indeed, Si crystallizes in the diamond, non-polar structure, while (Al,Ga)P materials crystallize in the polar zinc-blend structure. This difference in polarity leads to the apparition of anti-phase domains (APDs). The presence of such APDs is well-documented in the literature [7–9], and significant effort has been directed towards their suppression [2, 10]. As a result, GaP on quasi-exact (001) Si templates are now commercially available. These templates are free of dislocations, stacking-faults and possess an APD-free surface with excellent morphology [11].

In the present contribution, the use of these templates for the growth of GaP and AlGaP using metalorganic chemical vapor deposition (MOCVD) is investigated. Regrowth on these templates typically commences with a high-temperature annealing step in a phosphine ambient to remove the oxide that forms on top of the template. In the conditions developed by the present group of authors for the growth of high-quality, defect-free GaP and  $\text{Al}_{0.7}\text{Ga}_{0.3}\text{P}$  layers [12], this annealing step as well as the subsequent growth of AlGaP are carried out at  $850^\circ\text{C}$ . At this temperature, the lattice mismatch between GaP and Si increases to 0.53%. While the mismatch is still low, the critical layer thickness is bound to be exceeded during growth, leading to the relaxation of strain through the generation of misfit dislocations.

The objectives of the present paper are, therefore, to assess the mechanical stability of the GaP/Si template during high-temperature annealing and subsequent growth, and to evaluate the impact of any defects induced by plastic relaxation of misfit strain on the growth of AlGaP layers. The paper is structured as follows: a succinct description of the GaP/Si templates and the experiments

that were carried out is given first. The stability of GaP/Si templates during annealing and the efficiency of the annealing in removing the native oxide are then assessed for an array of temperatures. Finally, the impact that defects induced by the annealing have on the subsequent growth of GaP is discussed.

## 2. Experiment

A 200 mm GaP on Si template was purchased from NAsP<sub>III/V</sub> GmbH [11]. This template consists of 50 nm of GaP on 001 Si. The Si substrate is almost exact, with a small intentional miscut of  $0.18^\circ$  in  $[1\ 1\ 0]$ . According to Reference [2], this miscut, in conjunction with specific growth conditions, allows one to favor one crystal polarity over the other, resulting in a GaP/Si template with no observable APDs emerging at the GaP surface. Furthermore, given the small mismatch between GaP and Si - only 0.36% at room temperature - the GaP layer is pseudomorphically accommodated on the Si template and, therefore, contains very few dislocations. AFM images of the surface of GaP as received are shown in Figure 1. The surface exhibits step flow, with a root mean square (RMS) roughness of 0.2 nm and no visible defects in areas as large as  $10\ \mu\text{m}$  by  $10\ \mu\text{m}$ .

Cross-sections were prepared for observation in a transmission electron microscope (TEM). The cross-sections for transmission electron microscopy were prepared from some of the samples using Focused Ion Beam (FIB) ion milling and thinning. Prior to FIB ion milling, the sample surface was coated with 50 nm of carbon to protect the surface from the platinum mask deposited used for the ion milling process. Ion milling and thinning were carried out in a FEI SCIOS dual-beam FIB-SEM. Initial etching was performed at 30 keV, and final polishing was performed at 5 keV. All TEM cross-sections were observed in an aberration-corrected FEI TITAN 200 TEM-STEM operating at 200 keV. A high-angle annular dark-field image of the GaP/Si template is shown in Figure 2 (a). The image shows the presence of a 3 nm thick oxide layer on the surface of the 50 nm thick GaP layer. At this scale no defects are present in the GaP layer. Furthermore, 002 Dark-field TEM images of the samples confirm

that antiphase domains are indeed buried and do not emerge at the surface of the template - see Figure 2 (b). Nevertheless, misfit dislocations can be seen at the GaP/Si interface, as shown in the 220 Dark-field TEM image in Figure 2 (c). The grid has an approximate period of 1.5  $\mu\text{m}$ . The presence of this grid of dislocations, indicates the onset of plastic relaxation in the GaP/Si template, despite the small mismatch and relatively thin GaP layer. No threading dislocations are visible in the lamella, however. Given that the cross-sections are 25  $\mu\text{m}$  long by 80 nm wide, the threading-dislocation density is less than  $5 \times 10^7 \text{ cm}^{-2}$ .

[Figure 1 about here.]

The 200 mm template was diced into 50 mm wafers using laser cutting. Annealing and growth was carried out in a Veeco D180 Turbodisk reactor. The annealing experiments were carried out at three different annealing temperatures were used: 645 °C, 745 °C, and 845 °C, for 30 min in a phosphine ambient. The lowest temperature is close to the one disclosed in Reference [2], discussing the fabrication of the templates. The highest temperature is similar to one used for the obtained high quality GaP and AlGaP in Reference [12]. In addition to the annealing experiments, two samples were grown on the GaP/Si templates using MOCVD: a 200 nm GaP layer to test GaP growth, and, separately, the following structure to test AlGaP growth: a nominally 325 nm thick GaP buffer followed by two periods consisting of a 47 nm thick AlGaP layer, containing 73 at. % aluminum, and a 64 nm thick GaP layer. Additionally, the 80 nm of the GaP buffer contain five 1 nm thick AlP markers, spaced every 16 nm. Both samples were grown at a reactor temperature of 845 °C and a reactor pressure of 20 Torr, using trimethylaluminum, trimethylgallium, and phosphine as precursors to elementary aluminum, gallium, and phosphorous, respectively.

[Figure 2 about here.]

### 3. Results

The four AFM images in Figure 3 show the evolution of the surface morphology of the GaP/Si template as a function of temperature. At the lowest

annealing temperature, 645 °C, the GaP layer preserves its surface morphology, exhibiting step-flow and no visible defects. Nevertheless, the surface still exhibits spheres of oxide, indicating that the annealing temperature was not sufficient to completely remove the 3 nm oxide present at the surface of the template. Annealing for an hour at the same temperature did not yield any different results (not shown here). At higher temperatures, the oxide is completely removed and the step-flow morphology is still present, but the surface also exhibits stripes that are between 250 nm and 500 nm in width. At the highest annealing temperature, 845 °C, these stripes are more markedly present, creating a 3 nm high step. Additionally, several dislocations emerge at the surface of GaP, proof that the GaP layer plastically relaxes during the thermal annealing. The estimated threading-dislocation density is  $2 \times 10^8 \text{ cm}^{-2}$ , at least an order of magnitude higher than that present in the template initially.

[Figure 3 about here.]

The defects observed on the annealed samples persist in the 200 nm GaP layer grown on the GaP template, as shown the AFM images of the sample surface in Figure 4. The threading dislocation density, estimated from the density of pits in the AFM images, is  $2 \times 10^8 \text{ cm}^{-2}$ , no different than that observed for the sample at 845 °C. The GaP surface is also rougher owing to the onset of cross-hatch, with an RMS roughness of 0.9 nm, although step-flow is still preserved.

[Figure 4 about here.]

The defects observed in the GaP sample significantly perturb the growth of AlGaP, as revealed by the dark-field TEM images of the AlGaP sample, shown in Figure 5. These images reveal that the stripes observed already during annealing are bordered by pairs of micro-twins. When these cross the AlGaP layer, they induce severe faceting, mainly  $[1\ 1\ 2]$  and  $[1\ 1\ 4]$  planes. This faceting is mainly visible at the AlGaP/GaP interface. Subsequent growth of GaP tends to smooth this roughness, as seen at the second GaP/AlGaP interface in Figure 5, but the

surface becomes again rougher during the growth of the second AlGaP layer. The RMS roughness at the surface is 5 nm, more than an order of magnitude higher than the initial roughness of the template.

[Figure 5 about here.]

Finally, the GaP/Si interface now exhibits a dense misfit-dislocation grid, with an approximate period of 30 nm. Upon close inspection, this dislocation grid is composed up to 60 % of edge dislocations, and 40 % partial dislocations. Half of the partial dislocations at the interface combine with a Lomer-Cottrell dislocation in Si to form a stair-rod dislocation [13]. This type of defect is more common in highly mismatched systems, such as Ge/Si that has a lattice mismatch of 4%, an order of magnitude higher than GaP/Si [14], and to the extent of our knowledge has not been reported for lowly mismatched systems. The stair-rod itself appears as an inverted triangle at the GaP/Si interface. One such defect is shown in Figure 6 (a). Two apexes of the the triangle are partial misfit dislocations at the GaP/Si interface. Tracing the Burgers' circuits of the partial dislocations - Figures 6 (b) and (c) - reveals that their Burgers' vector is  $\mathbf{b} = \frac{1}{6}\mathbf{a}_{112}$ , in keeping with theory. Stacking faults extend from them and slip along [1 1 1] planes in Si until they meet at about 30 nm from the GaP/Si interface. There they combine to form the Lomer-Cottrell dislocation, that has a Burgers' vector of  $\mathbf{b} = \frac{1}{2}\mathbf{a}_{110}$  and is sessile.

[Figure 6 about here.]

#### 4. Discussion

Both AFM and TEM results show that the 50 nm GaP layer in the template does not contain any emerging APDs, and presents a smooth surface with a step-flow morphology and a roughness of only 0.2 nm. Nevertheless, the TEM images reveal that even at this thickness, which is lower than the critical thickness for plastic relaxation of GaP, reported at 90 nm [15], a loose misfit-dislocation grid is already present at the GaP/Si interface. In the literature, this has been

associated with thermal-stress induced relaxation of GaP during the cooling down phase of the GaP/Si template following GaP growth at temperatures higher than 400 °C. The reported threading dislocation densities in optimized conditions were of the order of  $1 \times 10^7 \text{ cm}^{-2}$  [16, 17], in agreement with the estimate obtained from TEM on the reference sample.

In two samples grown by MOCVD, the total GaP thickness is more than 250 nm, exceeding the critical thickness. In the literature full plastic relaxation of misfit strain that is due to lattice mismatch between GaP and Si is not achieved until a thickness of 200 nm [15, 17, 18]. At the reported thickness the samples are, therefore, fully plastically relaxed, and, accordingly, exhibit dislocation densities in the  $1 \times 10^8 \text{ cm}^{-2}$  range. The plastic relaxation of the strain induced to mismatch is further supported by the appearance of Lomer-Cottrell locks in Si. Indeed, the appearance of misfit dislocations in the Si substrate has been previously associated with the relaxation of strain that is due to the lattice mismatch, whereas thermal stress tends to generate defects at the GaP/Si interface or in GaP [16]. Although the RMS roughness of GaP sample increases, it still remains within reasonable limits, i.e. less than 1 nm. This roughness could be improved by increasing the V/III ratio and/or the reactor pressure.

The most cumbersome defects, however, are the micro-twins that already appear during high-temperature annealing of the GaP/Si template. These defects induce heavy faceting in the AlGaP layer, rendering these layers inappropriate for the growth of AlGaP/GaP Bragg mirrors. The micro-twins reported here are denser when the annealing temperature is increased. This result is contrary to what has been observed in the case of GaP grown on 4° off-cut Si using migration-enhanced molecular-beam epitaxy [19]. Indeed, in that reference, micro-twins are eliminated by implementing an annealing step after the initial nucleation of a 20 nm GaP layer. It is unclear whether the miscut is solely responsible for this difference, or whether the micro-twins could be annihilated by further tweaking of the growth and annealing conditions on the current templates. Alternatively, growth could be performed in a temperature range closer

to what has been reported by NAsP<sub>III/V</sub> GmbH., i.e. between 450 °C and 600 °C [2], using precursors that are better suited to low-temperature growth, such as triethylgallium and tri-tert-butylphosphine. Nevertheless, incorporation of high amounts of aluminum at low temperatures may prove challenging.

## 5. Conclusion

Despite excellent surface properties and the absence of emerging APDs, the GaP/Si templates used in the present contribution are revealed not to be compatible with the growth conditions developed of high-quality AlGaP and GaP growth on GaP substrates. Indeed, the templates are unstable at high temperatures, plastically relaxing to form micro-twins that detrimentally affects the growth of AlGaP in particular. Furthermore, the oxide layer present at the surface of the templates is not readily removed through annealing in a phosphine ambient at lower temperatures. A combination of wet etching to remove the oxide and growth with alternative metalorganic precursors that are better suited to low-temperature growth may be the only solution towards growth of high quality GaP and AlGaP on these templates.

## Acknowledgements

The authors would like acknowledge J. Nagle, A. De Rossi, and S. Combrié for their support and fruitful discussions. The authors thankfully acknowledge funding from the CNRS Renatech network and the ANR Labex TEMPOS (ANR-10-EQPX-0050).

## References

- [1] T. Soga, T. Jimbo, and M. Umeno. Dislocation generation mechanisms for gap on si grown by metalorganic chemical vapor deposition. *Applied Physics Letters*, 63:2543–2545, 1993.
- [2] A. Beyer, I. Németh, S. Liebich, J. Ohlmann, W. Stolz, and K. Volz. Influence of crystal polarity on crystal defects in gap grown on exact si (001). *Journal of Applied Physics*, 109:083529, 2011. doi: 10.1063/1.3567910.



- [3] Ioffe NSM archive. <http://www.ioffe.ru/SVA/NSM/Semicond/>. Accessed: 2020-08-12.
- [4] K. Hestroffer, D. Sperlich, S. Dadgostar, C. Golz, J. Krumland, W. T. Masselink, and F. Hatami. Transport properties of doped alp for the development of conductive alp/gap distributed bragg reflectors and their integration into light-emitting diodes. *Applied Physics Letters*, 112:192107, 2018.
- [5] J. S. Aitchinson, D. C. Hutchings, J.U. Kang, G. I. Stegeman, and A. Villeneuve. The nonlinear optical properties of algaas at the half band gap. *IEEE Journal of Quantum Photonics*, 33:341–348, 1997.
- [6] P. Colman, C. Husko, S. Combrié, I. Sagnes, and A. Wong, C. W. and De Rossi. Temporal solitons and pulse compression in photonic crystal waveguides. *Nature Photonics*, 4:864, 2010.
- [7] A. Beyer, J. Ohlmann, S. Liebich, H. Heim, G. Witte, W. Stolz, and K. Volz. Gap heteroepitaxy on si(001): Correlation of si-surface structure, gap growth conditions, and si-iii/v interface structure. *Journal of Applied Physics*, 111:083534, 2012.
- [8] P. Guillemé, M. Vallet, J. Stodolna, A. Ponchet, C. Cornet, A. Létoublon, P. Féron, O. Durand, Y. Léger, and Y. Dumeige. Antiphase domain tailoring for combination of modal and 4-quasi-phase matching in gallium phosphide microdisks. *Optics Express*, 24:14608, 2016.
- [9] I. Lucci, S. Charbonnier, L. Pedesseau, M. Vallet, L. Cerutti, J.B. Rodriguez, E. Tournié, R. Bernard, A. Létoublon, A. Bertru, N. Le Corre, S. Rennesson, F. Semond, G. Patriarce, L. Largeau, P. Turban, A. Ponchet, and C. Cornet. Universal description of iii-v/si epitaxial processes. *Physical Review Materials*, 2:060401(R), 2018.
- [10] I. Kunert, B. and Németh, S. Reinhard, K. Volz, and W. Stolz. Si (001)

surface preparation for the antiphase domain free heteroepitaxial growth of gap on si substrate. *Thin Solid Films*, 517:140–143, 2008.

- [11] Official NAsP website. <https://www.nasp.de/gap-on-si.html>. Accessed: 2020-08-13.
- [12] W. Xie, A. Martin, G. Beaudoin, I. Sagnes, F. Bretenaker, S. Combrié, F. Raineri, and A. De Rossi. Nonlinear, response of a gallium phosphide nanopatterned photonic waveguide in the cw regime. *Optics Letters*, 44: 2823–2826, 2019.
- [13] D. Hull and D. J. Bacon. *Introduction to Dislocations*. Elsevier, 5 edition, 2011. ISBN 978-0-08-096672-4.
- [14] R. J. Arroyo, G. Isa, F. and Isella, R. Erni, J. von Känel, P. Gröning, and D. M. Rossel. Effect of thermal annealing on the interface quality of ge/si heterostructures. *Scripta Materialia*, 170:52–56, 2019.
- [15] T. Soga, T. Jimbo, and M. Umeno. Initial stage of GaP/Si heteroepitaxial growth by metalorganic chemical vapor deposition. *Journal of Crystal Growth*, 163:163–170, 1996. doi: 10.1016/0022-0248(95)01046-7.
- [16] M. Tachikawa and H. Mori. Dislocation generation of GaAs on Si in the cooling stage. *Applied Physics Letters*, 55:2225, 1990. doi: 10.1063/1.102951.
- [17] J. M. Olson, M. M. Al-Jassim, A. Kibbler, and K. M. Jones. MOCVD Growth and Characterization of GaP on Si. *Journal of Crystal Growth*, 77: 515–523, 1986. doi: 10.1016/0022-0248(86)90346-5.
- [18] H. Emmer, C. T. Chen, R. Saive, D. Friedrich, Y. Horie, A. Arbabi, A. Faraon, and H. A. Atwater. Fabrication of Single Crystal Gallium Phosphide Thin Films on Glass. *Scientific Reports*, 7:4643, 2017. doi: 10.1038/s41598-017-05012-w.

- [19] K. Yamane, T. Kawai, Y. Furukawa, H. Okada, and A. Wakahara. Growth of low defect density gap layers on si substrates within the critical thickness by optimized shutter sequence and post-growth annealing. *Journal of Crystal Growth*, 312:2179–2184, 2010. doi: 10.1016/j.jcrysgro.2010.04.038.

**List of Figures**

1	(a) $100\ \mu\text{m}^2$ and (b) $4\ \mu\text{m}^2$ AFM images showing the surface of GaP on a GaP/Si template procured from NAsP <sub>III/V</sub> GmbH. Step-flow morphology is observed, with the step-flow occurring along the 001 direction. The RMS roughness is 0.2 nm. . . . .	14
2	(a) HAADF-STEM image of the as-received GaP/Si template. The image shows that the 50 nm thick GaP layer is covered by a 3 nm thick oxide layer. (b) 002 Dark-field TEM image showing the buried antiphase domains. In all the samples tested none of the domains emerge on the surface. (c) 220 Dark-field TEM image showing dislocations (black arrows) spaced by $1.5\ \mu\text{m}$ along the GaP/Si interface, indicating that despite the low mismatch and the relatively thin GaP layer, plastic relaxation has set on in the GaP/Si template . . . . .	15
3	$25\ \mu\text{m}^2$ AFM images of the surface of the GaP/Si template (a) before, and after annealing at (b) $645\ ^\circ\text{C}$ , (c) $745\ ^\circ\text{C}$ , and (d) $845\ ^\circ\text{C}$ for 30 min. At $645\ ^\circ\text{C}$ the atomic steps are preserved, but the surface is riddled with small pockets of oxide that was not removed. At higher annealing temperatures, these pockets disappear and the step-flow morphology is preserved. At $745\ ^\circ\text{C}$ and $845\ ^\circ\text{C}$ , however, bands that are on average 375 nm wide appear to rise above from the background. These are particularly visible in the sample annealed at $845\ ^\circ\text{C}$ . At this temperature the elevation of these bands is 5 nm. These bands are indicative of plastic relaxation taking place in the GaP layer of the template during high temperature annealing. . . . .	16
4	(a) $100\ \mu\text{m}^2$ and (b) $4\ \mu\text{m}^2$ AFM images of the GaP surface after the growth of a 200 nm of GaP on the GaP/Si template using MOCVD. Although step flow is still observed, the surface undulates along the $\langle 010 \rangle$ direction. This undulation is due to crosshatch. Crosshatch in GaP has been shown to occur anisotropically, more dense along the $\langle 010 \rangle$ direction than the $\langle 100 \rangle$ direction [9]. The surface is dotted by small pits where threading dislocations emerge, pointed out by white arrows in image (b). The threading dislocation density is estimated at $1 \times 10^8\ \text{cm}^{-2}$ , four orders of magnitude higher than that of the initial template. In addition to the emergence pits and the crosshatch, at least one 500 nm wide band delimited by two lines is pointed out by arrows in image (a), indicating that the bands that appear during annealing persist throughout subsequent growth of GaP. . . . .	17

5	<p>(a) 220 dark-field TEM image of the AlGaP/GaP structure grown on the GaP template. A dense grid of misfit dislocation is present at the GaP/Si interface, indicating that the structure is fully plastically relaxed. In addition to the dislocation grid, micro-twins appear in the structure. These often appear in pairs spaced by 365 nm, as revealed in (b) showing a 220 dark-field TEM image close up of one such pair. These pairs are linked to . These micro-twins induce faceting in AlGaP, significantly roughening the GaP/AlGaP interfaces. This faceting is highly detrimental to the optical properties of AlGaP/GaP pairs. As shown in Figure 3, these micro-twins already appear during the annealing of the GaP/Si template. . . . .</p>	18
6	<p>(a) HAADF-STEM image of a the GaP/Si interface in the AlGaP sample showing a stair-rod dislocation. The stair-rod forms at the junction of the stacking faults (<math>SF_1</math> and <math>SF_2</math>) that extend from two partial dislocations (<math>PD_1</math> and <math>PD_2</math>) at the GaP/Si interface and meet in the Si substrate, forming a sessile Lomer-Cottrell dislocation. (b,c) Insets showing magnified portions of the HAADF-STEM image in (a), centered around <math>PD_1</math> and <math>PD_2</math>, and their Burgers' circuits. . . . .</p>	19

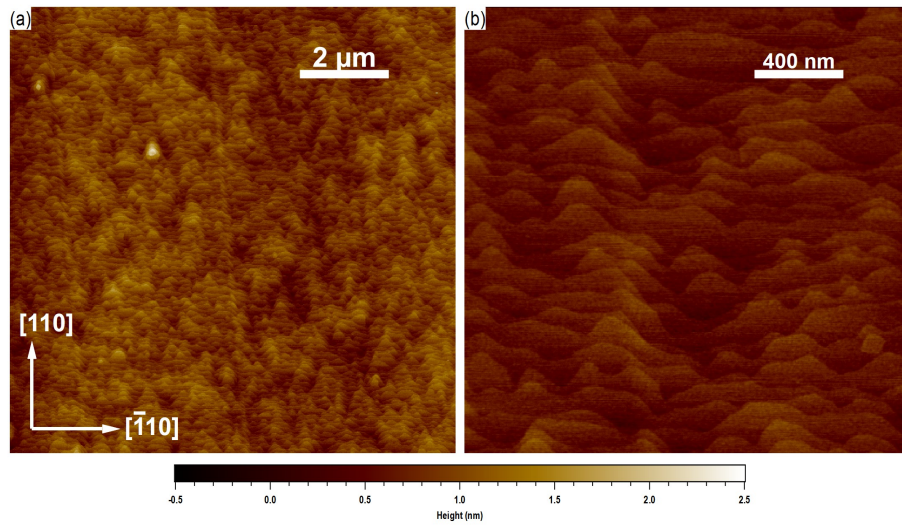


Figure 1: (a)  $100\ \mu\text{m}^2$  and (b)  $4\ \mu\text{m}^2$  AFM images showing the surface of GaP on a GaP/Si template procured from NAsP<sub>III/V</sub> GmbH. Step-flow morphology is observed, with the step-flow occurring along the 001 direction. The RMS roughness is 0.2 nm.

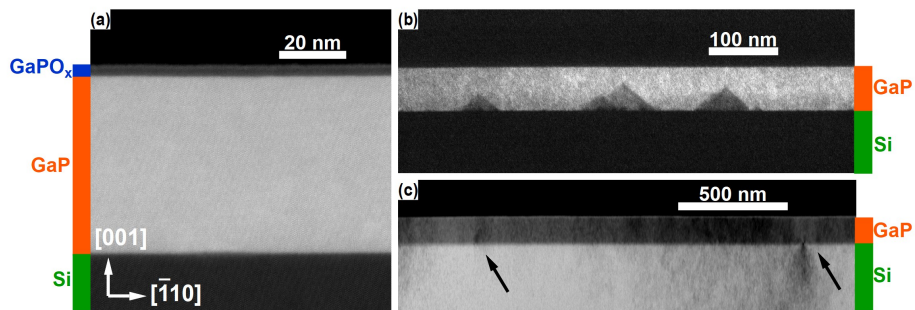


Figure 2: (a) HAADF-STEM image of the as-received GaP/Si template. The image shows that the 50 nm thick GaP layer is covered by a 3 nm thick oxide layer. (b) 002 Dark-field TEM image showing the buried antiphase domains. In all the samples tested none of the domains emerge on the surface. (c) 220 Dark-field TEM image showing dislocations (black arrows) spaced by 1.5  $\mu\text{m}$  along the GaP/Si interface, indicating that despite the low mismatch and the relatively thin GaP layer, plastic relaxation has set on in the GaP/Si template

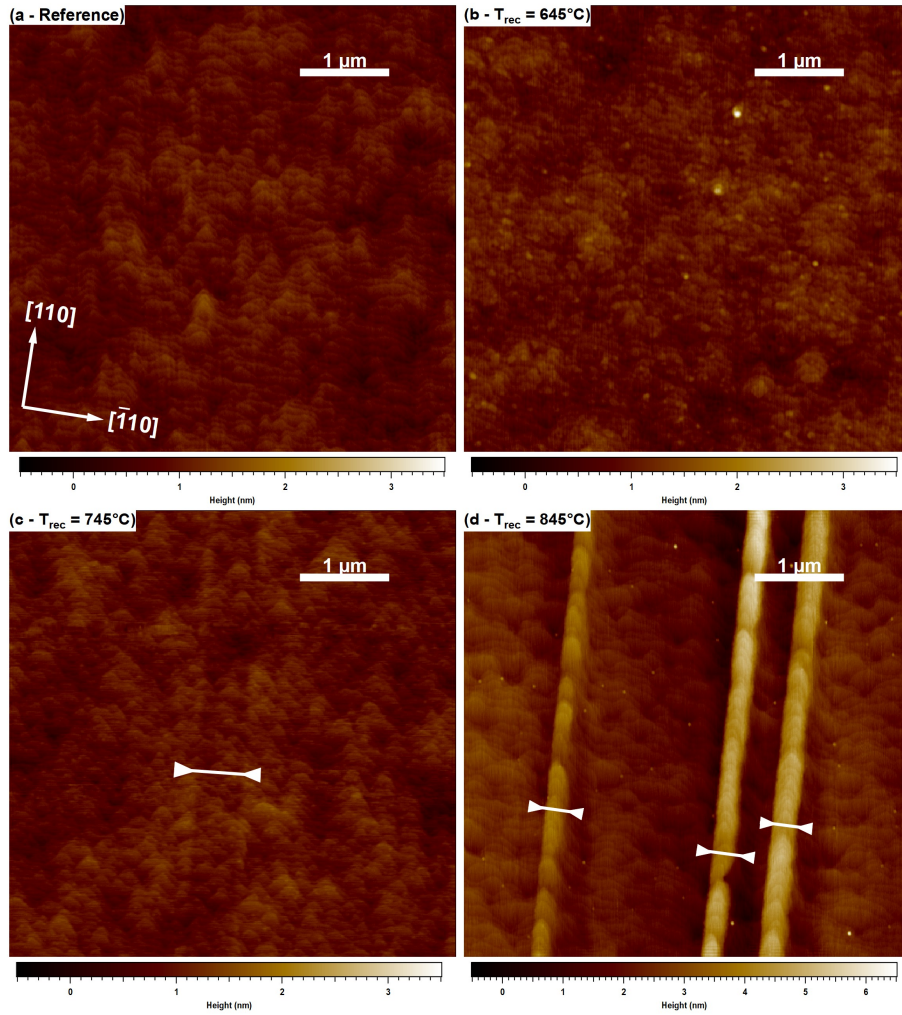


Figure 3:  $25 \mu\text{m}^2$  AFM images of the surface of the GaP/Si template (a) before, and after annealing at (b)  $645^\circ\text{C}$ , (c)  $745^\circ\text{C}$ , and (d)  $845^\circ\text{C}$  for 30 min. At  $645^\circ\text{C}$  the atomic steps are preserved, but the surface is riddled with small pockets of oxide that was not removed. At higher annealing temperatures, these pockets disappear and the step-flow morphology is preserved. At  $745^\circ\text{C}$  and  $845^\circ\text{C}$ , however, bands that are on average 375 nm wide appear to rise above from the background. These are particularly visible in the sample annealed at  $845^\circ\text{C}$ . At this temperature the elevation of these bands is 5 nm. These bands are indicative of plastic relaxation taking place in the GaP layer of the template during high temperature annealing.



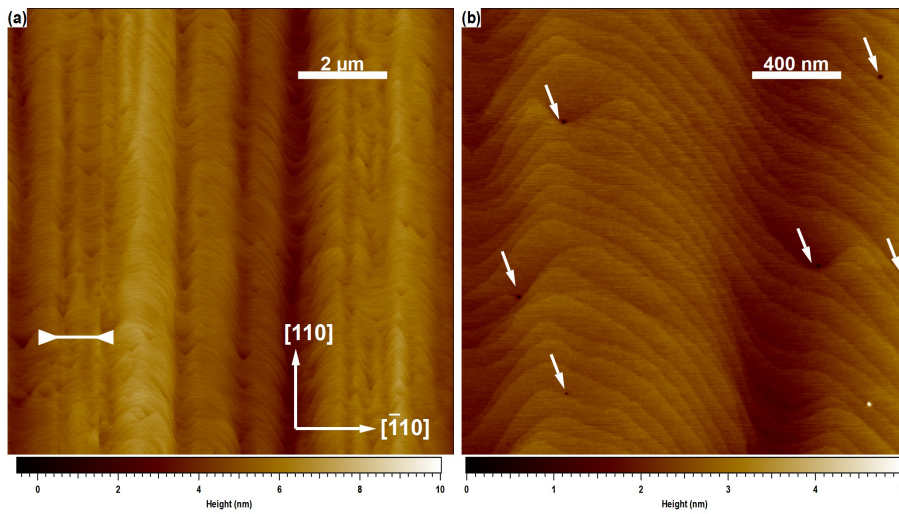


Figure 4: (a)  $100\ \mu\text{m}^2$  and (b)  $4\ \mu\text{m}^2$  AFM images of the GaP surface after the growth of a 200 nm of GaP on the GaP/Si template using MOCVD. Although step flow is still observed, the surface undulates along the  $\langle 010 \rangle$  direction. This undulation is due to crosshatch. Crosshatch in GaP has been shown to occur anisotropically, more dense along the  $\langle 010 \rangle$  direction than the  $\langle 100 \rangle$  direction [9]. The surface is dotted by small pits where threading dislocations emerge, pointed out by white arrows in image (b). The threading dislocation density is estimated at  $1 \times 10^8\ \text{cm}^{-2}$ , four orders of magnitude higher than that of the initial template. In addition to the emergence pits and the crosshatch, at least one 500 nm wide band delimited by two lines is pointed out by arrows in image (a), indicating that the bands that appear during annealing persist throughout subsequent growth of GaP.

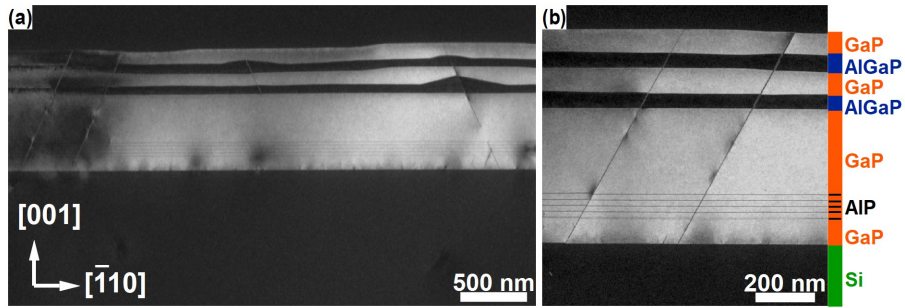


Figure 5: (a) 220 dark-field TEM image of the AlGaP/GaP structure grown on the GaP template. A dense grid of misfit dislocation is present at the GaP/Si interface, indicating that the structure is fully plastically relaxed. In addition to the dislocation grid, micro-twins appear in the structure. These often appear in pairs spaced by 365 nm, as revealed in (b) showing a 220 dark-field TEM image close up of one such pair. These pairs are linked to . These micro-twins induce faceting in AlGaP, significantly roughening the GaP/AlGaP interfaces. This faceting is highly detrimental to the optical properties of AlGaP/GaP pairs. As shown in Figure 3, these micro-twins already appear during the annealing of the GaP/Si template.

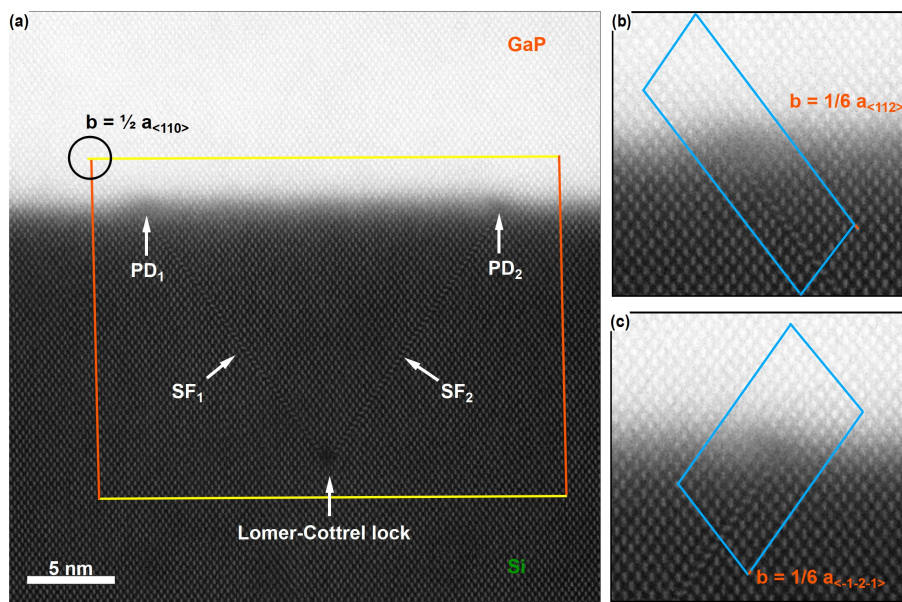


Figure 6: (a) HAADF-STEM image of a the GaP/Si interface in the AlGaP sample showing a stair-rod dislocation. The stair-rod forms at the junction of the stacking faults ( $SF_1$  and  $SF_2$ ) that extend from two partial dislocations ( $PD_1$  and  $PD_2$ ) at the GaP/Si interface and meet in the Si substrate, forming a sessile Lomer-Cottrell dislocation. (b,c) Insets showing magnified portions of the HAADF-STEM image in (a), centered around  $PD_1$  and  $PD_2$ , and their Burgers' circuits.